Ultramicroscopy 230 (2021) 113372

Contents lists available at ScienceDirect

Ultramicroscopy

journal homepage: www.elsevier.com/locate/ultramic

Transmission Kikuchi diffraction: The impact of the signal-to-noise ratio

Tomasz Tokarski [a,*], Gert Nolze [b], Aimo Winkelmann [a], Łukasz Rychłowski [a], Piotr Bała [c,a], Grzegorz Cios [a,*]

[a] Academic Centre for Materials and Nanotechnology, AGH University of Science and Technology, al. A. Mickiewicza 30, 30-059 Krakow, Poland
[b] Federal Institute for Materials, Research and Testing (BAM), Unter den Eichen 87, 12205 Berlin, Germany
[c] Faculty of Metals and Industrial Computer Science, AGH University of Science and Technology, al. A. Mickiewicza 30, 30-059 Krakow, Poland

ARTICLE INFO

Keywords:
EBSD
SEM
Transmission Kikuchi diffraction
Sample holder

ABSTRACT

Signal optimization for transmission Kikuchi diffraction (TKD) measurements in the scanning electron microscope is investigated by a comparison of different sample holder designs. An optimized design is presented, which uses a metal shield to efficiently trap the electron beam after transmission through the sample. For comparison, a second holder configuration allows a significant number of the transmitted electrons to scatter back from the surface of the sample holder onto the diffraction camera screen. It is shown that the secondary interaction with the sample holder leads to a significant increase in the background level, as well as to additional noise in the final Kikuchi diffraction signal. The clean TKD signal of the optimized holder design with reduced background scattering makes it possible to use small signal changes in the range of 2% of the camera full dynamic range. As is shown by an analysis of the power spectrum, the signal-to-noise ratio in the processed Kikuchi diffraction patterns is improved by an order of magnitude. As a result, the optimized design allows an increase in pattern signal to noise ratio which may lead to increase in measurement speed and indexing reliability.

1. Introduction

Scanning electron microscopy (SEM) offers unique possibilities for local, high-resolution microstructural analysis, including measurements on electron-transparent samples in transmission (STEM) [1]. For crystallographic characterization of thin samples, Transmission Kikuchi diffraction (TKD) can be used in the SEM [2,3], which achieves spatial resolution on the order of several nanometers (values from 2 nm to 5 nm are reported by various authors) [4–6]. This is an order of magnitude better in comparison to conventional electron backscatter diffraction (EBSD) which is used in a reflection mode [7].

In comparison to the conventional TKD solutions [2,3], a special measurement mode is provided by "on-axis" TKD [8], in which the phosphor screen is positioned horizontally under the sample, thereby increasing the measured intensity and minimizing gnomonic distortions. The original solutions rely on the standard, lateral positioning of the phosphor screen, which allows easy switching between EBSD and TKD modes. To distinguish between the two TKD setups, the conventional, lateral positioning of the detection screen will be referred to as "off-axis" TKD in the following.

Typical applications for the analysis of nanostructured, highly deformed, geological or corroded materials are discussed in [6]. Investigations of the influence of sample inclination angle, working distance (WD), sample thickness and electron acceleration voltage on the spatial resolution and quality of the measured TKD patterns show, for example, that higher acceleration voltages are advantageous for larger sample thicknesses [9–11]. Typical for the "off-axis" detector setup is the intensity gradient in the raw pattern, which, however, can be counteracted by varying the tilt angle of the sample between 0° to −40° [9].

Due to the low beam spread in electron-transparent samples, the highest spatial resolution is achieved with particularly thin samples in the order of a few tens of nanometers [9–13]. Thinner samples, however, also provide a lower total scattering signal, which significantly reduces the number of available electrons at large scattering angles, which are the dominating signal for "off-axis" TKD. For this reason, when measuring thin samples, it is particularly important to maximize the ratio between the useful diffraction signal and any additional background or noise. As has been discussed in [14], the mass-thickness will be a relevant parameter to compare TKD measurements done on different materials, where the optimum thickness depends on the material's

* Corresponding authors.
E-mail addresses: tokarski@agh.edu.pl (T. Tokarski), gert.nolze@bam.de (G. Nolze), winkelmann@agh.edu.pl (A. Winkelmann), rychlowski@agh.edu.pl (Ł. Rychłowski), pbala@agh.edu.pl (P. Bała), ciosu@agh.edu.pl (G. Cios).

https://doi.org/10.1016/j.ultramic.2021.113372
Received 15 April 2021; Received in revised form 27 July 2021; Accepted 5 August 2021
Available online 14 August 2021

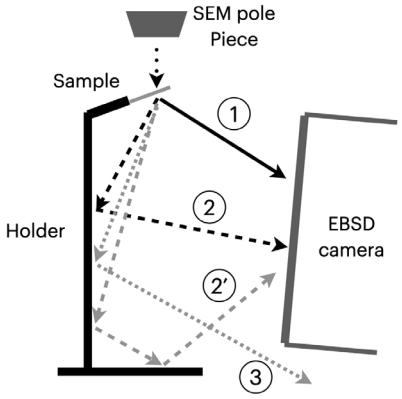

Fig. 1. Typical electron trajectories in TKD geometry, (1) electrons scattered from sample (useful signal), 2 and 2′ different routes of holder backscattered electrons, (3) electrons backscattered from the holder but not registered in EBSD detector.

density. As has also been shown for measurements on small particles in a backscatter geometry [15,16], the removal of background intensity has a crucial effect on the quality of the final Kikuchi diffraction pattern.

Previous TKD measurements on various metallic materials have shown that the design of the sample holder can play a key role for a reduction of background scattering [17–20]. Although descriptions of very different TKD specimen holders can be found in the literature [21–25], to our knowledge the specific influence of the holder design on the Kikuchi pattern quality has not been discussed in detail so far. In the current paper, we present a holder design which uses a metal shield to intercept transmitted electrons which are potentially re-scattered from the sample holder to the EBSD detector. We perform a detailed quantitative analysis of the signal-to-noise ratio in TKD patterns using their Fourier power spectrum and compare the results with those from a non-optimized holder. Using an analytical model for the background intensity and its noise, we show that after typical background removal by high-pass filtering of the raw image data, any high-frequency noise carried by the background necessarily will necessarily degrade the Kikuchi diffraction signal. In contrast, the improved holder design presented here acts as a blocking filter that removes electrons from the re-scattered background signal, which reduces the noise in the low-intensity Kikuchi diffraction signal and thus emphasizes the measured crystallographic information. As a result, the data acquisition speed can be increased, reducing negative effects such as sample contamination and drift.

2. Experimental and methods

Fig. 1 shows the three most typical electron trajectories for an "off-axis" TKD setup. Trajectory 1 describes the electrons which originate directly from the electron-transparent sample and represent the actually desired "useful signal". Trajectories 2 and 2′ represent all electrons which are backscattered one or multiple times from the holder or other surfaces in the SEM chamber and fall onto the screen. These electrons also contribute to the total signal registered by the camera. Since this signal comes mainly from the holder, it will be referred to as the "holder signal". Trajectory 3 represents all the electrons that do not fall on the fluorescent screen and can therefore be ignored here.

Diffraction patterns with a resolution of 480 × 480 pixels and color bit depth of 12-bits were collected with a Hikari (EDAX) EBSD detector. The detector was tilted by 5 degrees relatively to the optical direction of the beam. The field-emission scanning electron microscope (SEM) Versa 3D (FEI) was operated with an acceleration voltage of 30 kV

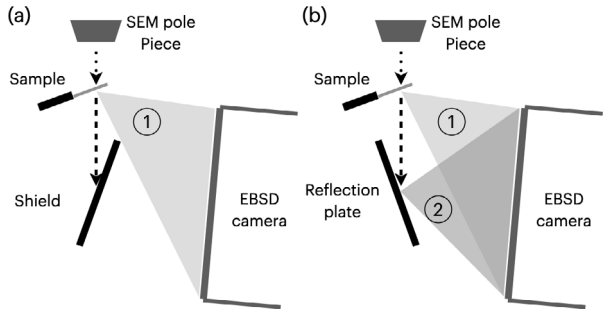

Fig. 2. Experimental TKD geometries: (a) Shield cuts off unwanted transmitted electrons, (b) Steel plate converts transmitted electrons into unwanted background. (1) Usable electron signal, (2) Background signal.

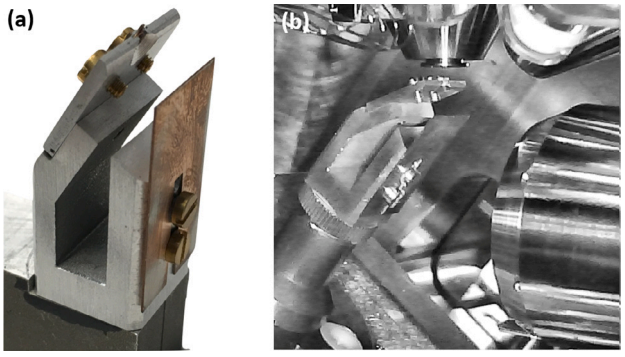

Fig. 3. Photos of the TKD measurement holder (pretilted by −60°) with installed additional shield: (a) general view, (b) setting in the measurement configuration of the microscope chamber (stage tilted by 40° to −20°).

and a beam current of ≈16 nA. All raw TKD patterns were stored for subsequent analysis.

Annealed AISI 316L steel (approx. chemical composition Fe-18Cr-10Ni-3Mo in wt.%) which was twin-jet electropolished using TenuPol-5 and A2 electrolyte (Struers) at 10 °C and 25 V, was investigated. The thickness of the sample used for the analysis was measured on a cross-section created by Focused Ion Beam milling with the Ga+ ions using Quanta 200i DualBeam apparatus (FEI). To measure specimen thickness, a thin foil surface was positioned perpendicularly to the ion beam, and the rectangular area of 30 × 5 μm was milled out. The longer edge of the area was set in the center of the TKD scan. In the next step thin foil was tilted 70° and images of the freshly revealed thin foil cross-section were acquired. Thickness measurement along foil cross-section was performed using ImageJ software, and results were corrected to compensate for the foil inclination.

Two experimental setups (see Fig. 2) were used to investigate the influence of the holder design on the signal of backscattered electrons for a common TKD geometry. An example of holder equipped with a shield used in the experiments is presented in Fig. 3.

The scenario outlined in Fig. 2(a) assumes that only electrons directly scattered from the sample are registered in the EBSD detector, while the scenario in Fig. 2(b) assumes that most of the electrons transmitted through the sample are backscattered by the flat holder tilted by 70° (i.e. at the typical EBSD sample angle) and reach the EBSD detector. The holder configurations shown in Fig. 2(a) and (b) are referred to as *shield* and *shield-less* configurations. A similar approach to the shield-less configuration has been used in the past for transmitted secondary electron conversion for STEM imaging in the SEM [26,27]. This plate can also be called a "transmission - backscatter conversion"

plate and can potentially be used for STEM imaging using the EBSD detector or using the FSD diodes mostly attached to the EBSD detector (as in [28]).

Three areas of the electron-transparent samples were measured. Thin (<50 nm) and thick foil (≈300 nm) areas were selected to illustrate the trade-off between signal intensity and spatial resolution: The highest spatial resolution is expected in the thin area, while the highest signal, however, is expected in moderately thick sample areas (thick enough to scatter electrons efficiently). The background electrons, which only come from the holder, were measured by directing the electron beam through the electropolished hole in the sample. This signal was taken as a reference for the limit of infinitesimally thin samples.

2.1. Kikuchi pattern power spectrum

The use of the Fourier transform allows us to analyze images in the frequency domain. The magnitude of the complex-valued Fourier spectrum is the power spectrum, which shows the relative weight of different spatial frequencies in an image [29]. Numerically, the power spectrum can be efficiently calculated by using the Fast Fourier Transform (FFT) [30].

In the context of EBSD, image quality measures based on the power spectrum of Kikuchi patterns have been proposed by Wilkinson [31] and Krieger Lassen [32,33]. FFT-based quality measures have the advantage that they are directly based on the image pixel intensities, i.e. independent of any detection of Kikuchi bands using the Radon transform and manufacturer specific definitions of "band slope", "band contrast", or "image quality", among others. Further examples for application of the FFT in EBSD include the feature extraction from Kikuchi patterns in the context of the Kikuchi bandlet method [34], image quality mapping in the context of a dictionary indexing approach [35], and the imaging of local deformations in materials [36].

In the following, all image processing by the FFT was carried out using the respective Python routines available in SciPy [37]. For the analysis of the raw EBSD patterns, we have applied the image processing procedure as described in [38] to obtain the Kikuchi diffraction signal. The procedure includes removal of detector effects via division by a background pattern coming from the holder. The holder background was obtained from a summation of diffraction-free images which were measured with the electron beam transmitted through the preparation hole in the sample. A dynamic correction of remaining low spatial frequencies (i.e. feature wavelengths larger than the observed Kikuchi band widths) are first removed by a local Gaussian kernel based FFT filter, with a spatial standard deviation of 5% of image width, as implemented e.g. by the SciPy function `scipy.ndimage.filters.gaussian_filter`. An additional global filtering was carried out by a 2D Gaussian high-pass filter on the power spectrum, with a full-width at half maximum (FWHM) of 0.004 cycles/pixel measured from the zero frequency position (i.e. the FWHM corresponds to 2 pixels near the center of the 2D FFT power spectrum). The aim of these filtering procedures is to discriminate the actual diffraction signal from any other intensity variation which are unrelated to the relevant Kikuchi diffraction effects [38] In order to reduce FFT artifacts which can result from the circular shape of the EBSD phosphor screen and the corresponding sharp circular edge in the image, we applied a Hanning window [30]. Finally, the high-pass filtered, windowed, pattern was normalized to a mean of 0.0 and a standard deviation of 1.0, which results in an average power of 1.0 per pixel in the FFT power spectrum, i.e. the squared values of all the pixels add up to the total number of pixels in the image after this normalization.

3. Results and discussion

3.1. Intensity on the EBSD detector

As mentioned above, the sample thickness is of crucial importance in TKD. A low interaction volume improves the spatial resolution, but has a negative effect on the intensity of the signal. In the "off-axis" TKD mode, the detector placed more to the side of the sample mainly detects the electrons scattered at a high angle, which greatly limits the intensity of the recordable signal.

Monte Carlo simulations performed with the software CASINO v3.3 show for a 50 nm thick stainless steel sample that 90% of the transmitted electrons are contained in a cone-shaped spatial segment with an aperture angle of only 12°, while only 1% are deflected into the sector covered by the EBSD screen. A significant portion of the transmitted electrons barely change direction and are found near the extended direction of the primary beam. This is one of the main reasons for the reduced performance of an "off-axis" TKD system. However, if the transmitted beam below the sample meets an improperly designed holder with its free surfaces facing the detector, this can lead to additional electrons scattering towards the screen, thereby creating an unwanted background.

To prepare the TKD sample, a metal foil was carefully thinned until hole formed centrally. With increasing distance to the hole, this results in a monotonic increase of thickness from 0 nm to 300 nm. Obtained thickness profile is presented in the top section of Fig. 3. To demonstrate the influence of the sample holder material on the intensity of the interfering background signal, both aluminum and stainless steel materials were used for the reflection plate. The resulting raw patterns are shown in Fig. 4. All raw images were taken under identical conditions, with the brightest diffraction image showing about 90% of the camera's saturation limit at maximum. For better comparison, the raw, unprocessed signal (left half) is overlaid with the background-corrected image (right half). The superimposed numbers describe the average pattern intensity in each case, where 0 would stand for no intensity and 1 would result in a completely saturated image.

The backscattered electron signal generated without any sample material (in the hole) is given in the left column (Fig. 4(a)) and shows in the top row the shielded case, as well as the results of two different plate materials in the middle (Al) and bottom row (stainless steel). As expected, the lowest average intensity of 0.005 is observed for the shielded case, where practically all electrons passing through the hole (or in the normal case through the sample) are blocked by the shield. If, on the other hand, the electrons are not blocked, the background adding to the sample diffraction pattern increases in accord with the increasing mean atomic number of the holder material, and the intensity maximum moves upwards in the image.

Usually, the angular distribution of electrons scattered in a thin foil is expected to show an intensity maximum at the bottom of the TKD patterns [4]. However, the shielded case (Fig. 4(b)) shows that the opposite is true for thin samples. A reversed intensity distribution with the intensity maximum in the upper region of the diffraction pattern is obviously caused by the electrons backscattered multiple times by the holder.

The intensity changes of the diffraction patterns for small sample thicknesses in Fig. 4(b) behave in principle similarly to the distributions in Fig. 4(a). The average intensity with shielding is still very low (0.008) and not visible to the eye (left half of the pattern). After brightness adjustment, however, the Kikuchi bands are clearly visible (right half of pattern). Patterns registered without shielding do show a clear increase in intensity. However, the diffraction signal is so small in relation to the intensity backscattered by the reflection plate that it becomes practically invisible. With increasing thickness of the foil, on the other hand, the proportion of the diffraction signal becomes larger (Fig. 4(c)), which on the one hand proves the clear increase in intensity and the lower noise for the shielded case, and on the

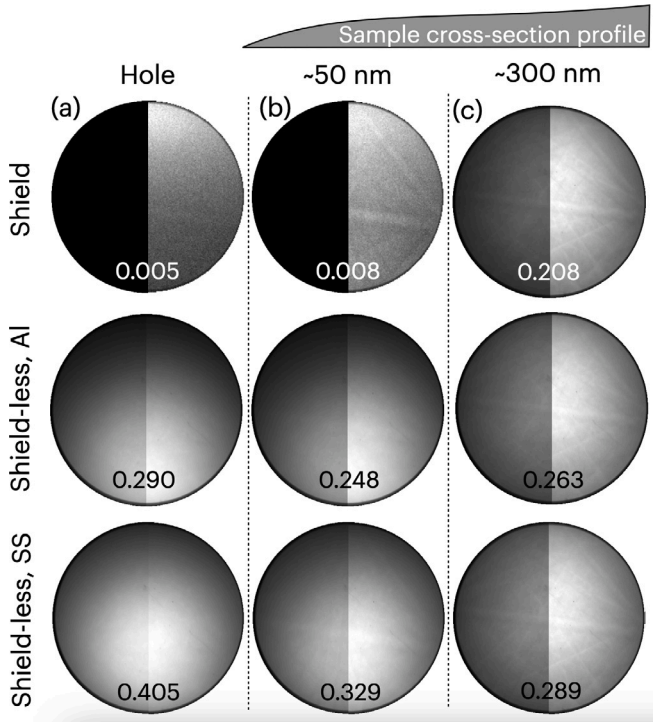

Fig. 4. Experimental raw TKD signals, shown on a common same gray scale range. Column (a), (b) and (c) shows patterns from the hole, thin (50 nm) and thick (300 nm) regions respectively. Rows upper, middle and lower are representing different holders setups with shield and two aluminum and stainless-steel (SS) reflector plate respectively. In each image, the left part is the raw signal while for the right part image histogram stretching was applied. Numbers are representing average signal intensity of images.

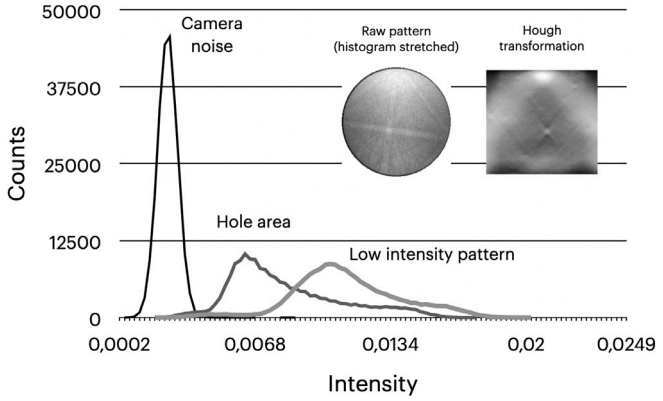

Fig. 5. Raw image histograms registered for the camera in the hole and thin foil region. As a reference, the blank signal acquired with the beam off is also presented.

other hand also explains the slightly amplified diffraction signal for the shield-less cases.

High-resolution measurements should actually be carried out on the thinnest available sample areas. However, due to the low interaction volume, the corresponding signal is then very low, so that the camera operates at the lower limit of its signal level. Extending the dwell time to compensate for the increased noise at low signal levels generally is not recommended, however, because of the negative effect on system stability due to beam and stage drift, and the risk of increasing carbon contamination. The shielding of all electrons not emitted by the actual interaction volume is therefore very important.

But how small can the diffraction signal be in order to correctly interpret a pattern in an "off-axis" TKD setup? To this end, Fig. 5 shows histograms derived from patterns recorded in the hole and in a region of the thin film. Both cases are compared with the camera noise registered when the electron beam was switched off. The histogram calculated from the blank camera image, which represents the electronic noise, has the maximum of the distribution at 0.0027 and practically ends at 0.006. The intensity of the shielded pattern, which is shown as inset together with its Hough transform in Fig. 5, is approximately three times more intense and delivers a histogram which practically starts at 0.011 with a maximum value at 0.02. The peaks in the Hough transform are clearly defined, proving that band detection can be effectively performed with only 2% of the camera maximum dynamic range.

An interesting case is given when the beam does not hit the sample at all (hole) and the signal from the reflecting plate is blocked by the shield. In comparison to the camera noise histogram, the resulting distribution is shifted towards higher values of even 0.005. This indicates that not all electron were blocked by the shield. It also proves the exceptional sensitivity of low intensity imaging of the camera used in the detector. Moreover, this indicates that even small variations in the detector design can influence the usable signal considerably, although it is invisible by the naked eye.

Even with additional backscattering, the non-shielded patterns can often result in indexable data after a suitable background correction. However, any signal contribution which is not exclusively coming from the interaction volume, has at least two negative effects: a lower acquisition speeds due to risk of the camera over-saturation, and a much lower signal-to-noise ratio. Especially the second factor is important since noise coming from the background signal of the holder cannot be discriminated from the noise of the original diffraction signal.

3.2. Analysis of the signal-to-noise ratio

In this section we will analyze how the signal-to-noise ratio (SNR) of the measured TKD patterns changes when they are measured for different background conditions. The Fourier transformation of the observed diffraction patterns is used to characterize the SNR for an experimental setup with the beam shield in operation in comparison to a situation with additional, detrimental, rescattering of the transmitted beam towards the EBSD detector.

In Fig. 6, we compare the results of the Kikuchi pattern image processing for measurements from a 50 nm thin region of an austenite sample. The pattern in the right column of Fig. 6 was measured in the shield-less configuration, the pattern in the left column was measured at the same sample position, but with the shield set properly in operation instead. As can be seen on power spectra, the processed Kikuchi diffraction pattern which was obtained in the presence of additional rescattering shows higher noise compared to the pattern taken with the shield configuration.

When the transmitted beam is properly dumped into the sample holder, the total intensity of the raw EBSD pattern measured was only about 15% of the intensity when the additional rescattering was introduced by the aluminum reflection plate below the sample. (the position of the beam was in column 190 in the maps shown in Fig. 7). However, the noise in the resulting, processed Kikuchi pattern is significantly lower when it is measured with the shield to minimize any additional rescattering. Thus, the rescattered intensity is detrimental to the diffraction-signal-to-noise ratio in the final Kikuchi pattern, because, as we will discuss below, the rescattered intensity contributes to additional noise counts, while it does not contain any Kikuchi diffraction signal at the same time.

As can be seen in the 2D power spectra in Fig. 6(c) and (d), the outer regions corresponding to the highest frequencies show the presence of white noise (frequency independent), while the high intensity

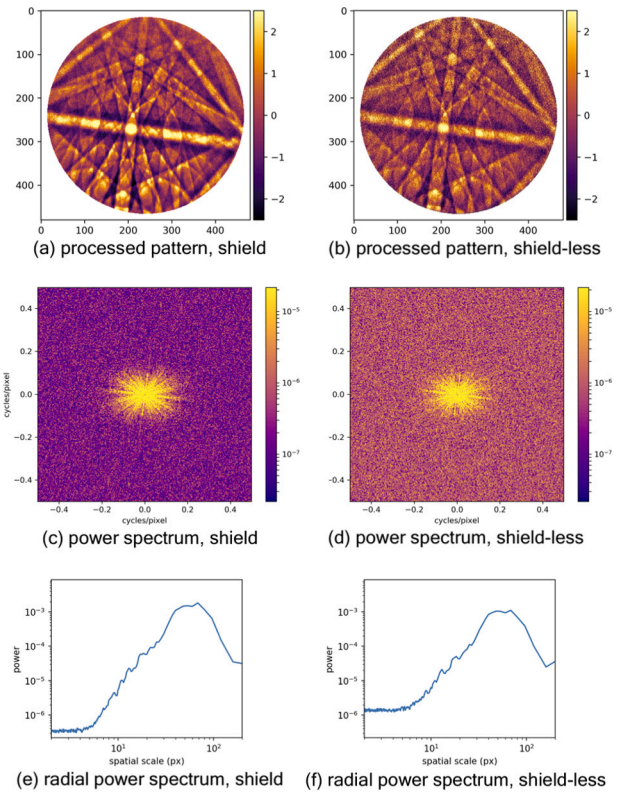

Fig. 6. Processed Kikuchi patterns of austenite (a, b, top row), 2D FFT power spectra (c, d, middle row), and the radial power spectrum intensity shown in dependence on the spatial length scale (e, f, bottom row). The left column shows the results for shield configuration, the right column shows the result including additional rescattering from an aluminum plate below the sample. The sample thickness for both measurements was about 50 nm.

central part correspond to the spatial frequencies of the Kikuchi pattern features.

In order to characterize the relative contribution of the different spatial frequencies in a Kikuchi pattern irrespective of the direction of the wave vector, we calculated the azimuthal average of the 2D power spectra [32,39], which we show as a function of the spatial scale of features (i.e. corresponding to the wavelength of periodic features). These radial power spectra are shown in Fig. 6(e) and (f), where dominating part of intensity is in the spatial wavelengths of a few tens of pixels which correspond to dimension of the Kikuchi bands. The white noise can be identified by the nearly horizontal part of the radial power distribution shown for smallest spatial length scales in Fig. 6(e) and (f). For the pattern measured with an adequate shielding, this noise level is at 3.5×10^{-7}, while the rescattered intensity increases the noise level to about 1.5×10^{-6}, i.e. by more than a factor of 4.

3.2.1. Role of the background intensity in reducing the signal-to-noise ratio

As we have seen in Fig. 6, the processed Kikuchi patterns show a substantial improvement in the signal-to-noise ratio if the diffraction-less background signal is removed prior to detection. The reduction of noise occurs despite the fact that the raw EBSD pattern shows a significantly lower total signal when the beam is shielded. This observation indicates that, even though the background signal is not contributing to any Kikuchi features, it still contributes to the noise in the processed Kikuchi pattern.

A basic analytic treatment can be developed by considering the various contributions to signal and noise which originate from the Kikuchi diffraction signal on the one hand and from a background signal on the other hand. In relation to the Kikuchi signal, we assume that the background signal is characterized as showing only smooth variations on the scale of the Kikuchi diffraction features.

Quantitatively, the observed total electron counts T at a point on the phosphor screen can be divided into the background part B (being the sum of the holder background and the specimen signal background), which changes only slowly with pixel position on the screen (and which thus can be filtered out by image processing techniques), and a Kikuchi diffraction part K, which contributes to the actual Kikuchi diffraction features:

$$T = B + K \tag{1}$$

If the mean total signal in a pixel corresponds to a number of T electrons, then the number of noise counts N_T is defined via the standard deviation of T, which is $\sqrt{T}$ for counts distributed according to the Poisson distribution [40]:

$$N_T = \sqrt{T} \tag{2}$$

The ratio of the noise counts relative to the total signal is given by:

$$\frac{N_T}{T} = \frac{\sqrt{T}}{T} = \frac{1}{\sqrt{T}} \tag{3}$$

In order to obtain the actual Kikuchi signal, the image processing removes only the mean background signal from the total counts. This is possible because of the smooth spatial variations of the background. The pixel-wise noise of the background signal, however, cannot be discriminated from the pixel-wise noise of the Kikuchi signal and thus cannot be filtered by image post-processing. The influence of the background signal on the Kikuchi signal-to-noise ratio is thus due to the background noise counts $N_B = \sqrt{B}$.

As a result, the noise counts N_T due to the counts of the *total* signal will appear in the Kikuchi diffraction signal after image processing, not only the respective noise counts $\sqrt{K}$ specific to the Kikuchi counts K:

$$N_K = N_T = \sqrt{K + B} = \sqrt{K(1 + b)} \tag{4}$$

where b is the relative number of background counts with respect to the number of Kikuchi counts as $B = b \cdot K$. This is why, with an increasing number of background counts, also the relative noise of the processed Kikuchi pattern increases:

$$\frac{N_K}{K} = \frac{\sqrt{K(1 + b)}}{K} = \frac{\sqrt{(1 + b)}}{\sqrt{K}} \tag{5}$$

The background increases the effective noise counts N_K after image processing without affecting the useful Kikuchi counts K.

From this equation, we can estimate that for a relative background signal in the order of $b = 3 \ldots 8 \ldots 13$, the processed Kikuchi pattern noise increases by factors of $\sqrt{(1 + b)} = 2 \ldots 3 \ldots 4$ relative to the Poisson limit of $1/\sqrt{K}$. These estimated increases in noise are consistent with the observed increase by a factor of more than 4 in the power of the high-frequency spatial variations in the power spectrum, as was discussed in the previous section for the power spectra of Fig. 6.

3.2.2. Relative signal-to-noise ratio in maps

In order to discuss a consistent signal-to-noise ratio for different Kikuchi patterns in a map, we define the signal as the portion of the power in the central region ranging up to wave numbers of $k = 0.3$ cycles per pixel and we consider the power in the remaining higher frequencies as the power of the noise, see Fig. 6.

In Fig. 7, we show the total intensity and the signal-to-noise ratio for a TKD map of an austenite sample, measured approximately in a stripe perpendicular to a hole, which is seen on the right edge of the map. The map shows increasing thicknesses from right to left, with the maximum thickness slightly below 300 nm at the left edge. As can be seen from the maps of the total intensities, the map for the aluminum rescattering

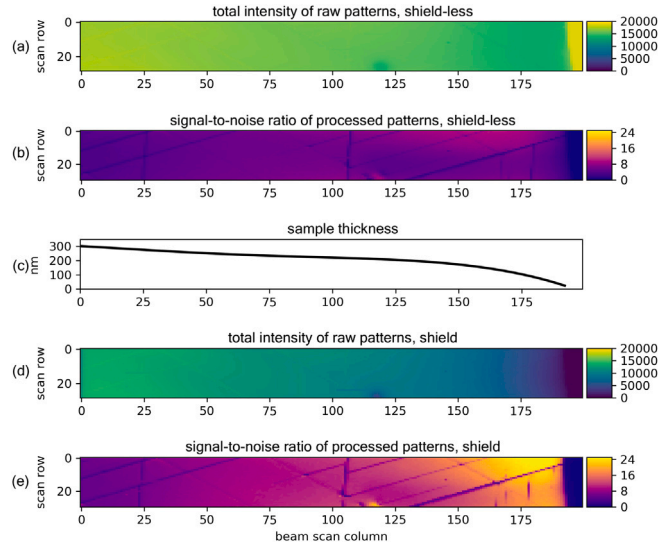

Fig. 7. Relative change of the signal-to-noise ratio (SNR) in the Kikuchi diffraction patterns with additional, detrimental, rescattering, compared to measurements with an adequate shielding. (a) total intensity in the raw TKD patterns with rescattering from aluminum, (b) SNR with rescattering (c) sample thickness as a function of the beam position (d) total intensity in the raw TKD patterns with the shield, (e) SNR with the shield. The SNR is calculated from the power spectrum of the Kikuchi diffraction patterns as explained in the text. The maximum SNR in the thin sample region shows values near 26 with the shield installed, which is reduced to values near 10 due to the rescattered electrons. The step size in the map is 0.1 μm.

plate in Fig. 7(a) shows an overall higher background intensity as compared to the blocked beam in Fig. 7(d).

The thickness-dependent signal-to-noise ratios as defined by the relative parts of intensity inside and outside of $k = 0.3$ in the power spectrum are shown in Fig. 7(b) and (e). The optimum signal-to-noise ratio is observed for the low thicknesses in Fig. 7(e), where the additional background due to multiple inelastic scattering in the sample is still low. This observation is consistent with thickness-dependent studies of "on-axis" TKD [10]. For sample thicknesses larger than presented here, a decrease of the total intensity is expected due to inelastic scattering processes.

In a study of the depth resolution of TKD [41], Liu et al. estimated that the diffraction signal originate form the bottom layer of the foil, with depth corresponding to the mean free path of thermal diffuse scattering events. At the same time, the ideal sample thickness for TKD analysis should be in the order of about 20 times the elastic scattering mean free path for samples of high crystal symmetry. Approximating the situation in austenite, we consider the value of 7.8 nm for the elastic mean free path in Cu at 30 kV [42], which is near to Fe in the periodic table. The corresponding ideal thicknesses would then be $\lessapprox$200 nm for our measurements of Fe samples. This estimation agrees with the measured thicknesses of our sample, which we show by the curve in Fig. 7(c).

The measurements with rescattered intensity from the transmitted beam show a decreased signal-to-noise ratio in Fig. 7(b). This observation indicates that the sample holder with an efficient shield is improving the signal-to-noise ratio relative to measurements with a less efficient prevention of the rescattering of the transmitted beam. For the largest thicknesses, the SNR of both measurements begins to be similar, which we assign to the multiple elastic and inelastic scattering processes which contribute to an increased background intensity but not to the diffraction signal [38,43,44]

As we have shown, the additional noise in the processed Kikuchi patterns is due to a background which does not contribute a diffraction signal. The Kikuchi pattern image post-processing can only remove the mean slowly-varying background intensity but not the pixel-wise background noise. In effect, any additional background counts make it necessary to measure more total counts in order to obtain the same relative noise with respect to the final, image-processed, Kikuchi signal. This is why it is very effective to block those specific electrons which only contribute to the background, before they can deteriorate the signal-to-noise ratio in the detection process. For the same incident beam current, this would allow less exposure times, or the detection of weaker diffraction features. In addition to the physical blocking of the transmitted beam, as demonstrated here, a background removal would be also possible by energy-filtering of Kikuchi patterns [45]. Energy filtering would have the advantage to additionally remove the specific background contribution which is created by multiple inelastic scattering in the sample itself and which thus cannot be removed by the beam dump. Such background filtering would be especially relevant to conventional EBSD in a reflection geometry, but also for the thicker regions of the TKD sample shown in Fig. 7, away from the observed maximum of the signal-to-noise ratio.

4. Summary and conclusions

The signal-to-noise ratio in "off-axis" TKD measurements strongly depends on the number of electrons which are scattered back from other parts than the sample, notably from the sample holder. In the present work, we used two extreme configurations for illustration of the influence of re-scattering effects: a holder with a shield cutting off all electrons which are backscattered from other parts than the sample, and a holder with reflecting plate which directed a significant part of the transmitted electrons towards the EBSD detector screen.

The extreme forward-directed anisotropy of the differential electron scattering cross section within an electron transparent sample results in low numbers of detected electrons at the relatively large scattering angles corresponding to directions on the EBSD phosphor screen. The majority of electrons pass through the sample nearly unaffected in the forward direction, and can subsequently hit the sample holder or other surfaces in the SEM chamber, potentially scattering back towards the detector screen. While this superimposed signal increases the intensity of the raw TKD signal, the quality of the actual diffraction information is significantly deteriorated by the collateral noise introduced by the re-scattered electrons.

The experiments discussed above showed that an optimal measurement setup can be achieved if the secondary, re-scattered signal is blocked by a suitable shield. This shielding is especially efficient for low-intensity diffraction of electrons, in particular for very thin samples and/or for low atomic number materials such as Al and Mg with small atomic scattering cross sections. Quantitatively, it was shown that the power spectra of the processed Kikuchi patterns showed up to 5-fold lower noise for the shielded design.

The shielding of the secondary scattering has clear advantages when using high beam currents, as the risk of oversaturation of the EBSD detector is noticeably lower.

When scanning materials with medium atomic numbers (Cu, Fe, Ni), measurement speeds comparable to those of standard EBSD could be achieved with shielding (100 to 200 patterns per second for a Hikari detector and pattern sizes of 120 × 120 pixels). For lower atomic number materials (e.g. Mg or Al), the speed drops, however, to about half due to the smaller intensity of large angle scattering of electrons.

In summary, the increased acquisition speed could be used employing the shielded holder design leading to possibly significant reduction of drift problems and carbon contamination compared to the unshielded design.

Declaration of competing interest

The authors declare that they have no known competing financial interests or personal relationships that could have appeared to influence the work reported in this paper.

Acknowledgments

The research is financed by the Polish National Science Centre UMO-2016/21/B/ST8/01183 and 2020/37/B/ST5/03669 and by the Polish National Agency for Academic Exchange grant no. PPI/APM/2018/1/00049/U/001 and no. PPN/ULM/2019/1/00068 /U/00001.

References

[1] T. Klein, E. Buhr, C.G. Frase, TSEM: A review of scanning electron microscopy in transmission mode and its applications, in: Advances in Imaging and Electron Physics, Elsevier, 2012, pp. 297–356, http://dx.doi.org/10.1016/b978-0-12-394297-5.00006-4.

[2] R. Keller, R. Geiss, Transmission EBSD from 10 nm domains in a scanning electron microscope, J. Microsc. 245 (3) (2012) 245–251, http://dx.doi.org/10.1111/j.1365-2818.2011.03566.x.

[3] P.W. Trimby, Orientation mapping of nanostructured materials using transmission kikuchi diffraction in the scanning electron microscope, Ultramicroscopy 120 (2012) 16–24, http://dx.doi.org/10.1016/j.ultramic.2012.06.004.

[4] N. Brodusch, H. Demers, R. Gauvin, Nanometres-resolution kikuchi patterns from materials science specimens with transmission electron forward scatter diffraction in the scanning electron microscope, J. Microsc. 250 (1) (2013) 1–14, http://dx.doi.org/10.1111/jmi.12007.

[5] N. Brodusch, H. Demers, M. Trudeau, R. Gauvin, Acquisition parameters optimization of a transmission electron forward scatter diffraction system in a cold-field emission scanning electron microscope for nanomaterials characterization, Scanning 35 (6) (2013) 375–386, http://dx.doi.org/10.1002/sca.21078.

[6] G.C. Sneddon, P.W. Trimby, J.M. Cairney, Transmission kikuchi diffraction in a scanning electron microscope: A review, Mater. Sci. Eng.: R: Rep. 110 (2016) 1–12, http://dx.doi.org/10.1016/j.mser.2016.10.001.

[7] A.J. Schwartz, M. Kumar, B.L. Adams, D.P. Field (Eds.), Electron Backscatter Diffraction in Materials Science, Springer US, 2009, http://dx.doi.org/10.1007/978-0-387-88136-2.

[8] J.J. Fundenberger, E. Bouzy, D. Goran, J. Guyon, H. Yuan, A. Morawiec, Orientation mapping by transmission-SEM with an on-axis detector, Ultramicroscopy 161 (2016) 17–22, http://dx.doi.org/10.1016/j.ultramic.2015.11.002.

[9] S. Suzuki, Features of transmission EBSD and its application, JOM 65 (9) (2013) 1254–1263, http://dx.doi.org/10.1007/s11837-013-0700-6.

[10] E. Brodu, E. Bouzy, J.-J. Fundenberger, Diffraction contrast dependence on sample thickness and incident energy in on-axis transmission kikuchi diffraction in SEM, Ultramicroscopy 181 (2017) 123–133, http://dx.doi.org/10.1016/j.ultramic.2017.04.017.

[11] J.-W. Shih, K.-W. Kuo, J.-C. Kuo, T.-Y. Kuo, Effects of accelerating voltage and specimen thickness on the spatial resolution of transmission electron backscatter diffraction in Cu, Ultramicroscopy 177 (2017) 43–52, http://dx.doi.org/10.1016/j.ultramic.2017.01.020.

[12] E. Brodu, E. Bouzy, A new and unexpected spatial relationship between interaction volume and diffraction pattern in electron microscopy in transmission, Microsc. Microanal. 24 (6) (2018) 634–646, http://dx.doi.org/10.1017/s1431927618015441.

[13] E. Brodu, S.D. Jadhav, K. Vanmeensel, M. Seefeldt, Determination of the structure and orientation of nanometer-sized precipitates in matrix materials via transmission diffraction signals emitted by bulk samples in the scanning electron microscope, Mater. Charact. 166 (2020) 110454, http://dx.doi.org/10.1016/j.matchar.2020.110454.

[14] K. Rice, R. Keller, M. Stoykovich, Specimen-thickness effects on transmission Kikuchi patterns in the scanning electron microscope, J. Microsc. 254 (3) (2014) 129–136, http://dx.doi.org/10.1111/jmi.12124.

[15] J.A. Small, J.R. Michael, Phase identification of individual crystalline particles by electron backscatter diffraction, J. Microsc. 201 (2001) 59–69.

[16] J.A. Small, J.R. Michael, D.S. Bright, Improving the quality of electron backscatter diffraction (EBSD) patterns from nanoparticles, J. Microsc. 206 (2002) 170–178.

[17] T. Tokarski, G. Cios, A. Kula, P. Bała, High quality transmission Kikuchi diffraction analysis of deformed alloys - Case study, Mater. Charact. 121 (2016) 231–236, http://dx.doi.org/10.1016/j.matchar.2016.10.013.

[18] Y. Zhao, S. Wroński, A. Baczmański, L.L. Joncour, M. Marciszko, T. Tokarski, M. Wróbel, M. François, B. Panicaud, Micromechanical behaviour of a two-phase Ti alloy studied using grazing incidence diffraction and a self-consistent model, Acta Mater. 136 (2017) 402–414, http://dx.doi.org/10.1016/j.actamat.2017.06.022.

[19] G. Cios, T. Tokarski, P. Bała, Strain-induced martensite reversion in 18cr–8ni steel – transmission kikuchi diffraction study, Mater. Sci. Technol. 34 (5) (2018) 580–583, http://dx.doi.org/10.1080/02670836.2017.1376456.

[20] G. Cios, T. Tokarski, A. Zywczak, R. Dziurka, M. Stepien, L. Gondek, M. Marciszko, B. Pawlowski, K. Wieczerzak, P. Bala, The investigation of strain-induced martensite reverse transformation in aisi 304 austenitic stainless steel, Metall. Mater. Trans. A 48 (10) (2017) 4999–5008, http://dx.doi.org/10.1007/s11661-017-4228-1.

[21] R. van Bremen, D.R. Gomes, L. de Jeer, V.O. k, J.D. Hosson, On the optimum resolution of transmission-electron backscattered diffraction (t-EBSD), Ultramicroscopy 160 (2016) 256–264, http://dx.doi.org/10.1016/j.ultramic.2015.10.025.

[22] H. Yuan, E. Brodu, C. Chen, E. Bouzy, J.-J. Fundenberger, L. Toth, On-axis versus off-axis transmission kikuchi diffraction technique: application to the characterisation of severe plastic deformation-induced ultrafine-grained microstructures, J. Microsc. 267 (1) (2017) 70–80, http://dx.doi.org/10.1111/jmi.12548.

[23] N. Mortazavi, M. Esmaily, M. Halvarsson, The capability of transmission Kikuchi diffraction technique for characterizing nano-grained oxide scales formed on a FeCrAl stainless steel, Mater. Lett. 147 (2015) 42–45, http://dx.doi.org/10.1016/j.matlet.2015.02.008.

[24] C.D. Judge, W. Li, C. Mayhew, A. Buyers, G.A. Bickel, Adopting Transmission kikuchi diffraction to characterize grain structure and texture of Zr-2.5Nb candu pressure tubes, CNL Nucl. Rev. 7 (1) (2018) 119–125, http://dx.doi.org/10.12943/CNR.2017.00010.

[25] W. Zieliński, T. Płociński, K. Kurzydłowski, Transmission kikuchi diffraction and transmission electron forescatter imaging of electropolished and FIB manufactured TEM specimens, Mater. Charact. 104 (2015) 42–48, http://dx.doi.org/10.1016/j.matchar.2015.04.003.

[26] U. Golla, B. Schindler, L. Reimer, Contrast in the transmission mode of a low-voltage scanning electron microscope, J. Microsc. 173 (3) (1994) 219–225, http://dx.doi.org/10.1111/j.1365-2818.1994.tb03444.x.

[27] L. Reimer, B. Volbert, Detector system for backscattered electrons by conversion to secondary electrons, Scanning 2 (4) (1979) 238–248.

[28] S.I. Wright, M.M. Nowell, R. de Kloe, P. Camus, T. Rampton, Electron imaging with an EBSD detector, Ultramicroscopy 148 (2015) 132–145, http://dx.doi.org/10.1016/j.ultramic.2014.10.002.

[29] W. Burger, M.J. Burge, Principles of Digital Image Processing. Core Algorithms, Springer London, 2009, http://dx.doi.org/10.1007/978-1-84800-195-4.

[30] W.H. Press, S.A. Teukolsky, W.T. Vetterling, B.P. Flannery, Numerical Recipes: The Art of Scientific Computing, third ed., Cambridge University Press, New York, NY, USA, 2007, URL https://books.google.de/books?id=1aAOdzK3FegC.

[31] A.J. Wilkinson, D.J. Dingley, Quantitative deformation studies using electron back scatter patterns, Acta Metall. Mater. 39 (12) (1991) 3047–3055, http://dx.doi.org/10.1016/0956-7151(91)90037-2.

[32] N.C. Krieger Lassen, Automated Determination of Crystal Orientations from Electron Backscattering Patterns (Ph.D. thesis), Technical University of Denmark, 1994, p. 136.

[33] N.C. Krieger Lassen, D. Juul Jensen, K. Condradsen, Automatic recognition of deformed and recrystallized regions in partly recrystallized samples using electron back scattering patterns, Mater. Sci. For. 157–162 (1994) 149–158, http://dx.doi.org/10.4028/www.scientific.net/msf.157-162.149.

[34] F. Ram, S. Zaefferer, D. Raabe, Kikuchi bandlet method for the accurate deconvolution and localization of kikuchi bands in kikuchi diffraction patterns, J. Appl. Cryst. 47 (1) (2014) 264–275, http://dx.doi.org/10.1107/s1600576713030446.

[35] K. Marquardt, M.D. Graef, S. Singh, H. Marquardt, A. Rosenthal, S. Koizuimi, Quantitative electron backscatter diffraction (EBSD) data analyses using the dictionary indexing (DI) approach: Overcoming indexing difficulties on geological materials, Amer. Mineral. 102 (9) (2017) 1843–1855, http://dx.doi.org/10.2138/am-2017-6062.

[36] M.D. Borcha, S.V. Balovsyak, I.M. Fodchuk, V.Y. Khomenko, O.P. Kroitor, V.N. Tkach, Local deformation in diamond crystals defined by the fourier transformations of kikuchi patterns, J. Superhard Mater. 35 (5) (2013) 284–291, http://dx.doi.org/10.3103/s1063457613050031.

[37] P. Virtanen, R. Gommers, T.E. Oliphant, M. Haberland, T. Reddy, D. Cournapeau, E. Burovski, P. Peterson, W. Weckesser, J. Bright, S.J. van der Walt, M. Brett, J. Wilson, K. Jarrod Millman, N. Mayorov, A.R.J. Nelson, E. Jones, R. Kern, E. Larson, C. Carey, I. Polat, Y. Feng, E.W. Moore, J. Vand erPlas, D. Laxalde, J. Perktold, R. Cimrman, I. Henriksen, E.A. Quintero, C.R. Harris, A.M. Archibald, A.H. Ribeiro, F. Pedregosa, P. van Mulbregt, S... Contributors, Scipy 1.0: Fundamental algorithms for scientific computing in python, Nat. Methods 17 (2020) 261–272, http://dx.doi.org/10.1038/s41592-019-0686-2.

[38] A. Winkelmann, T.B. Britton, G. Nolze, Constraints on the effective electron energy spectrum in backscatter kikuchi diffraction, Phys. Rev. B 99 (2019) 064115, http://dx.doi.org/10.1103/PhysRevB.99.064115.

[39] E.W. Koch, E.W. Rosolowsky, R.D. Boyden, B. Burkhart, A. Ginsburg, J.L. Loeppky, S.S.R. Offner, TurbuStat: Turbulence statistics in python, Astron. J. 158 (1) (2019) 1, http://dx.doi.org/10.3847/1538-3881/ab1cc0.

[40] J.R. Taylor, Introduction to Error Analysis: The Study of Uncertainties in Physical Measurements, University Science Books, 1997, URL http://www.worldcat.org/oclc/34150960.

[41] J. Liu, S. Lozano-Perez, A.J. Wilkinson, C.R.M. Grovenor, On the depth resolution of transmission Kikuchi diffraction (TKD) analysis, Ultramicroscopy 205 (2019) 5–12, http://dx.doi.org/10.1016/j.ultramic.2019.06.003.

[42] L. Reimer, Scanning Electron Microscopy - Physics of Image Formation and Microanalysis, second ed., Springer Verlag, Berlin Heidelberg New York, 1998, http://dx.doi.org/10.1007/978-3-540-38967-5.

[43] A. Winkelmann, K. Aizel, M. Vos, Electron energy loss and diffraction of backscattered electrons from silicon, New J. Phys. 12 (2010) 053001, http://dx.doi.org/10.1088/1367-2630/12/5/053001.

[44] M. Vos, A. Winkelmann, Effects of multiple elastic and inelastic scattering on energy-resolved contrast in kikuchi diffraction, New J. Phys. 21 (12) (2019) 123018, http://dx.doi.org/10.1088/1367-2630/ab5cd1.

[45] S. Vespucci, A. Winkelmann, G. Naresh-Kumar, K.P. Mingard, D. Maneuski, P.R. Edwards, A.P. Day, V. O'Shea, C. Trager-Cowan, Digital direct electron imaging of energy-filtered electron backscatter diffraction patterns, Phys. Rev. B 92 (2015) 205301, http://dx.doi.org/10.1103/PhysRevB.92.205301.